

International Journal of Applied Mechanics
Vol. 5, No. 3 (2013) 1350031 (20 pages)
© Imperial College Press
DOI: 10.1142/S1758825113500312



THERMALLY INDUCED VIBRATIONS OF SOLAR PANEL AND THEIR COUPLING WITH SATELLITE

ZHENXING SHEN and GENGKAI HU*

*Key Laboratory of Dynamics and Control of Flight Vehicle
Ministry of Education, School of Aerospace Engineering
Beijing Institute of Technology
Beijing 100081, P. R. China
hugeng@bit.edu.cn

Received 3 February 2013

Revised 7 April 2013

Accepted 20 April 2013

Published

A coupled thermal-structural model of a laminated composite plate is proposed by using the absolute nodal coordinate formulation, the transverse shear and normal deformations through element thickness are included. The dynamic equations of structure are established by applying the d'Alembert's principle and then solved numerically to determine dynamic responses and transient heat conduction in the structure due to the nonlinear elastic force and thermal radiation. A cantilevered flexible solar panel subjected suddenly to a solar radiation is examined, it is found that by considering the coupling between the thermal and structural responses, thermal flutter of the composite panel can be well predicted. The coupled behavior of the composite solar panel with a satellite is also analyzed by idealizing it as a rigid-flexible multibody system in the low earth orbit, in which a natural coordinate formulation is established to analyze the attitude of the satellite rigid hub, the thermal snap phenomenon is also well predicted.

Keywords: Thermally induced vibrations; thermal flutter; thermal snap; absolute nodal coordinate formulation; natural coordinate formulation.

1. Introduction

Spacecraft usually has large and flexible appendages connected with its main platform. When it enters into or exits from eclipse, thermally induced vibrations (TIVs) may take place due to rapid heat flux change on the flexible appendages. In the sunlight region, solar radiation will lead to a cross-sectional temperature gradient in the appendage, consequently resulting in thermo-elastic deformation and structural motion. Particularly, TIVs may occur more easily in the low earth orbit due to orbital transition time, for examples, the OGO (Orbiting Geophysical Observatories) series satellites experienced such failure in the 1960s [Thornton and Foster, 1992], the Hubble Space Telescope (HST) observed a pointing "jitter" after launch

*Corresponding author.

Z. Shen & G. Hu

(April 1990) [Thornton and Foster, 1992], and the Upper Atmosphere Research Satellite (UARS) experienced attitude disturbances (September 1991) [Woodard, 1998]. In addition, thermal flutter and thermal snap were also observed on the HST and the UARS, respectively. Thermal flutter is an unstable TIVs response [Thornton and Foster, 1992] with an increasing amplitude, and thermal snap is a quasi-static TIVs response with a rapid and non-oscillatory deformation [Johnston and Thornton, 2000]. Therefore, TIVs problems are detrimental to spacecraft operation and should be considered in spacecraft design.

To address the TIVs problem, Boley and Barder [1957] considered the inertia effect on structural response of a simply supported isotropic rectangular plate subjected to a rapid heating. Thereafter, the TIVs of different plates [Biswas, 1978; Tauchert, 1989; Chang *et al.*, 1992; Tran *et al.*, 2007] and material property [Gupta and Singhal, 2010] were examined. Additionally, Brischetto [2009] studied the thermal stress problem of thick and thin multilayered cylindrical and spherical shells, and Lal and Singh [2010] examined the second-order statistics of thermal buckling response of shear deformable laminated composite plate. When large flexible appendages are mounted on the satellite, the TIVs of the appendages will be coupled with motion of the satellite. In order to evaluate this coupling behavior, Bainum *et al.* [1989] analyzed the response of large space structures subjected to thermal shock, and Zimelman *et al.* [1991] examined the effect of thermal torque on the TOPEX satellite during eclipse transitions. Johnston and Thornton [1998, 2000] performed an analysis of TIVs for a simple satellite with flexible solar panel, and the UARS was also examined to explain the change of the satellite attitude during eclipse transitions. However, these works neglected the coupling between thermal and structural responses. In fact, the structural deformation will alter the heat absorption from structure surface, and this thermal-structural coupling is the origin of the unstable TIVs (thermal flutter) of the structures [Thornton and Foster, 1992]. Li *et al.* [2007] studied the nonlinear vibration of practical thin-walled large-scale space structures due to thermal loading, and established the criterion of thermal flutter. To this end, Xue *et al.* [2007] developed a finite element scheme to solve the thermally induced bending-torsion coupling vibration of thin-walled beams, and the thermal and structure coupling is taken into account. However, the coupling between thermal and structural responses of solar panel structure and their influence on vibration response of satellite have not been addressed yet.

In this paper, we will employ the absolute nodal coordinate formulation (ANCF) and the natural coordinate formulation (NCF) to characterize the coupling between the thermal and structural responses of solar panel, as well as coupling between the TIVs of solar panel and the motion of satellite. The ANCF, proposed by Shabana [1996], can accurately describe large deformation and motion of flexible bodies. In addition, the mass matrix remains constant, which is extremely advantageous to solve dynamic problems. It should be mentioned that practically at the same time, Zhu *et al.* [Zhu and Morrow, 1998; Zhu and Pour, 2010] proposed a nodal position

finite element method (NPFEM) which was similar to the existing ANCF. The NCF is introduced by García de Jalón *et al.* [1986, 1987] for spatial systems, in which global position vectors of basic points and global unit vectors are used as nodal coordinates, therefore the mass matrix is also constant in the formulation. In this paper, we will combine the ANCF and the NCF to describe the dynamic response of a rigid-flexible multibody system subjected to thermal shock during eclipse transitions. The paper is arranged as the following: the theoretical formation for coupled thermal and structural responses based on the ANCF is explained in Sec. 2, examples are also provided in this section to illustrate the method. The formulation to characterize the coupling between solar panel and satellite is detailed in Sec. 3, in which the dynamic responses of a satellite with solar panel in the low earth orbit are also simulated for ellipse transition, finally some conclusions are given in Sec. 4.

2. Coupled Thermal and Structural Formulations

2.1. Theoretical analysis

In this section, we will examine the coupled thermal and structural responses for a solar panel subjected to thermal shock during eclipse transitions. A 3D laminated composite plate element under thermal effect will be established by using the ANCF. To this end, a flexible plate i is divided into elements, as shown in Fig. 1(a). For the element j shown in Fig. 1(b), there are four nodes j_1, j_2, j_3, j_4 and 48 degrees of freedom in the ANCF, twelve at each node. In Fig. 1, the Cartesian coordinate systems \mathbf{XYZ} and \mathbf{xyz} are the inertial coordinate systems for the whole plate and the element j , respectively.

The position vector \mathbf{r} of an arbitrary point on the mid-plane of the element j belonging to the laminate composite plate i is defined as [Mikkola and Shabana, 2003].

$$\mathbf{r}^{i,j}(x, y, z, t) = \begin{bmatrix} r_1^{i,j} \\ r_2^{i,j} \\ r_3^{i,j} \end{bmatrix} = \mathbf{S}(x, y, z) \mathbf{e}^{i,j}(t), \quad (1)$$

where $\mathbf{S}(x, y, z)$ is the matrix of shape function for the plate element, and x, y, z are the element coordinates. In the element coordinate system, the shape functions are independent of time. The laminated plate element model is assumed to have transverse shear and normal deformations through the thickness. Therefore, the matrix of the shape function can be written as

$$\mathbf{S}(x, y, z) = [S_1 \mathbf{I} \quad S_2 \mathbf{I} \quad \cdots \quad S_{16} \mathbf{I}], \quad (2)$$

where \mathbf{I} is the 3×3 identity matrix.

Z. Shen & G. Hu

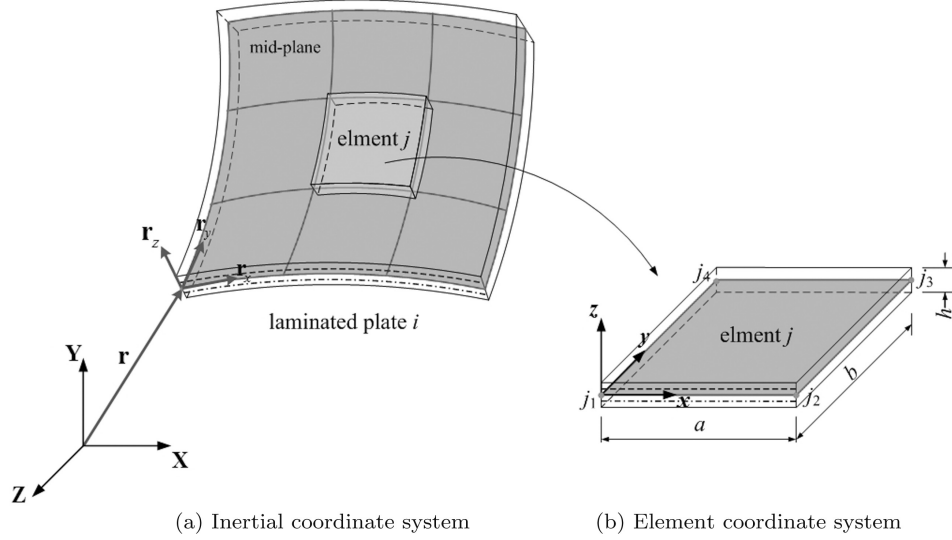


Fig. 1. Laminated composite plate element of ANCF.

In the ANCF, the nodal coordinate vector for the node j_1 on the element j belonging to the flexible plate i is defined as

$$\mathbf{e}^{i,j_1} = [\mathbf{r}^{i,j_1^T} \quad \mathbf{r}_x^{i,j_1^T} \quad \mathbf{r}_y^{i,j_1^T} \quad \mathbf{r}_z^{i,j_1^T}]^T, \quad (3)$$

where \mathbf{r}^{i,j_1} is the global position vector of the node j_1 , and the others are the global slope vectors at the node j_1 . The vector of nodal coordinates on the midplane of the element j belonging to the plate i can be written as

$$\mathbf{e}^{i,j} = [\mathbf{e}^{i,j_1^T} \quad \mathbf{e}^{i,j_2^T} \quad \mathbf{e}^{i,j_3^T} \quad \mathbf{e}^{i,j_4^T}]^T. \quad (4)$$

For efficient computation of elastic force in the ANCF, the condensed shape vector is used [Gerstmayr and Shabana, 2005]

$$\bar{\mathbf{S}}(x, y, z) = [S_1 \quad S_2 \quad \cdots \quad S_{16}]^T \quad (5)$$

and the change matrix of nodal coordinates is given by [Gerstmayr and Shabana, 2005]

$$\bar{\mathbf{e}}^{i,j} = [\bar{\mathbf{e}}^{i,j_1^T} \quad \bar{\mathbf{e}}^{i,j_2^T} \quad \bar{\mathbf{e}}^{i,j_3^T} \quad \bar{\mathbf{e}}^{i,j_4^T}]^T, \quad (6)$$

where $\bar{\mathbf{e}}^{i,j_1}$ is the change matrix of nodal coordinates for the node j_1 , it is written as

$$\bar{\mathbf{e}}^{i,j_1} = [\mathbf{r}^{i,j_1} \quad \mathbf{r}_x^{i,j_1} \quad \mathbf{r}_y^{i,j_1} \quad \mathbf{r}_z^{i,j_1}]^T. \quad (7)$$

Thus, the position vector can be written finally as

$$\mathbf{r}^{i,j}(x, y, z, t) = \bar{\mathbf{e}}^{i,j}(t)\bar{\mathbf{S}}(x, y, z). \quad (8)$$

To derive the dynamic equations, the mass matrix and the element elastic force of an element will be evaluated based on the position vector \mathbf{r} . Thus, the mass matrix

of the element j can be defined as [Shabana, 2005]

$$\mathbf{M}^{i,j} = \int_0^a \int_0^b \int_{-\frac{h}{2}}^{\frac{h}{2}} \rho^{(k)} \mathbf{S}^T \mathbf{S} \, dx dy dz, \quad (9)$$

where $\mathbf{M}^{i,j}$ is a constant matrix, and $\rho^{(k)}$ is the material density of the k th layer in the laminate plate. The virtual work of the internal elastic force is evaluated by [Shabana, 2008]

$$\delta W_s = - \int_V \boldsymbol{\sigma}_{P1} : \delta \mathbf{J} dV = - \int_V \boldsymbol{\sigma}_{P2} : \delta \boldsymbol{\varepsilon} dV = - \int_V \mathbf{J} \boldsymbol{\sigma}_{P2} : \delta \mathbf{J} dV = \mathbf{Q}^T \delta \mathbf{e}, \quad (10)$$

where $\boldsymbol{\sigma}_{P1}$ is the first Piola–Kirchhoff stress tensor, $\boldsymbol{\sigma}_{P2}$ is the second Piola–Kirchhoff stress tensor, and \mathbf{J} is the matrix of the position vector gradient

$$\mathbf{J} = \frac{\partial \mathbf{r}}{\partial \mathbf{r}_0} = \frac{\partial \mathbf{r}}{\partial \mathbf{x}} \frac{\partial \mathbf{x}}{\partial \mathbf{r}_0} = \bar{\mathbf{e}}^T \frac{\partial \bar{\mathbf{S}}}{\partial \mathbf{x}} \cdot \left(\frac{\partial \mathbf{S}}{\partial \mathbf{x}} \mathbf{e}_0 \right)^{-1}, \quad (11)$$

where \mathbf{r}_0 is the initial position vector, and the coordinate $\mathbf{x} = [x \ y \ z]^T$, $\boldsymbol{\varepsilon}$ is the Green-Lagrange strain tensor

$$\boldsymbol{\varepsilon} = \frac{1}{2} (\mathbf{J}^T \mathbf{J} - \mathbf{I}) \quad (12)$$

and \mathbf{Q} is the internal elastic force. The elastic force matrix of the element j is defined as

$$\mathbf{Q}^{i,j,T} = - \int_0^a \int_0^b \int_{-\frac{h}{2}}^{\frac{h}{2}} \mathbf{J}^{i,j} \boldsymbol{\sigma}_{P2}^{i,j,(k)} : \frac{\partial \mathbf{J}^{i,j}}{\partial \mathbf{e}^{i,j}} dx dy dz, \quad (13)$$

where $\boldsymbol{\sigma}_{P2}^{i,j,(k)}$ is the second Piola–Kirchhoff stress tensor of the k th layer [Reddy, 2004],

$$\boldsymbol{\sigma}_{p2}^{i,j,(k)} = \mathbf{C}^{i,j,(k)} : (\boldsymbol{\varepsilon}^{i,j} - \boldsymbol{\varepsilon}_T^{i,j,(k)}), \quad (14)$$

where $\mathbf{C}^{i,j,(k)}$ is the elastic constant of the k th layer, and

$$\boldsymbol{\varepsilon}_T^{i,j,(k)} = \boldsymbol{\alpha}^{i,j,(k)} \cdot \Delta T^{i,j}(x, y, z, t), \quad (15)$$

where $\boldsymbol{\alpha}^{i,j,(k)}$ is the coefficient of thermal expansion of the k th layer, and

$$\Delta T^{i,j}(x, y, z, t) = T^{i,j}(x, y, z, t) - T_0^{i,j}(x, y, z, t_0), \quad (16)$$

where T_0 is a reference or initial temperature, and T is the current temperature. In this paper, the current temperature T will be obtained by solving the transient heat conduction equation with help of the finite element method, which will be explained in Sec. 2.3.1.

According to the d'Alembert's principle, the dynamic equation of the element j is finally derived as

$$\mathbf{M}^{i,j} \ddot{\mathbf{e}}^{i,j} + \mathbf{Q}^{i,j} = \mathbf{0}. \quad (17)$$

Z. Shen & G. Hu

2.2. Numerical validation

To verify the proposed laminate composite plate element with thermal effect based on the ANCF, a composite plate made of graphite/epoxy laminates is examined in a static case, and the results will be compared with those obtained by ANSYS commercial finite element software. For simplicity, the plate is assumed to be clamped at the AD edge, as shown in Fig. 2, and a uniform temperature increase 10K is imposed, i.e., $\Delta T(x, y, z, t) = 10\text{ K}$. The geometry and material property of a graphite/epoxy layer are listed in Table 1 [Tauchert, 1989]. The plate is made up of four graphite/epoxy layers, as shown in Fig. 2, two stacking sequences $[0^\circ/90^\circ/90^\circ/0^\circ]$ and $[0^\circ/90^\circ/0^\circ/90^\circ]$ are examined. The property of the composite plate is obtained by laminate theory.

Figure 3 shows the Z -displacements of the point B on the laminated plate, obtained by using the proposed laminated plate element based on the ANCF and the ANSYS shell99 element, respectively. Different meshing: 4×4 , $5 \times 5 \dots 16 \times 16$

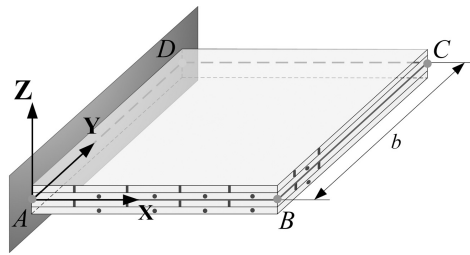


Fig. 2. Cantilevered graphite/epoxy laminate.

Table 1. Geometry and material property of a graphite/epoxy layer.

Property	Graphite/epoxy layer
Length $AB = BC$	0.254 m
Thickness h	6.35×10^{-4} m
Density ρ	1.6036×10^{-3} kg/m ³
Young's modulus	
E_{11}	1.3790×10^{11} N/m ²
E_{22}	8.9635×10^{11} N/m ²
E_{33}	8.9635×10^{11} N/m ²
Shear modulus	
G_{12}	7.10185×10^9 N/m ²
G_{13}	7.10185×10^9 N/m ²
G_{23}	3.44750×10^9 N/m ²
Poisson's ratio	
$\nu_{12} = \nu_{13} = \nu_{23}$	0.3
Coefficient of thermal expansion (CTE)	
α_{11}	-3.006×10^{-7} /K
α_{22}	2.8080×10^{-5} /K
α_{33}	2.8080×10^{-5} /K

rectangular elements are examined, it is shown that the proposed element model agrees well with the ANSYS shell99 element.

For further comparison, Fig. 4 shows the Z-displacement of the edge *BC* at the midplane of the $[0^\circ/90^\circ/0^\circ/90^\circ]$ laminated plate, again evaluated by the current element and the ANSYS shell99 element. The 8×8 rectangular element is used, it is shown that the current ANCF element agrees well with the prediction by the ANSYS shell99 element.

2.3. TIVs response of a cantilevered solar panel

2.3.1. *Thermal analysis of laminated composite plate*

A laminated plate is assumed to be subjected to a thermal shock induced by solar radiation in space environment. Thermal analysis model of the plate is illustrated

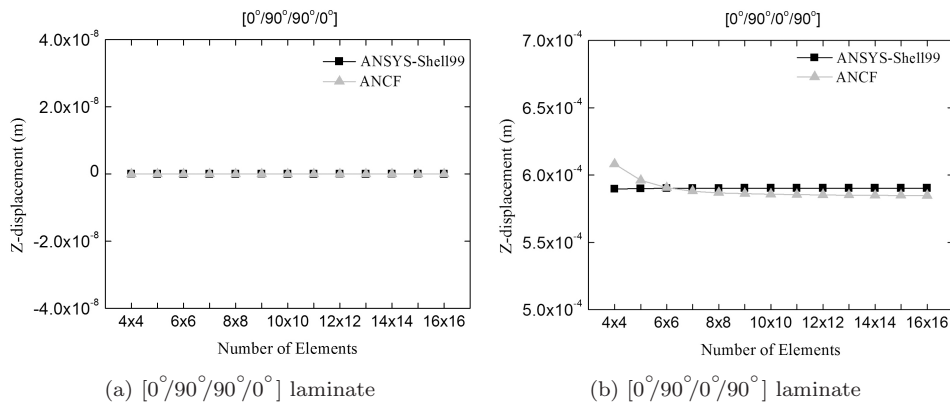


Fig. 3. Z-displacement at the point *B* of the laminate under a uniform thermal loading.

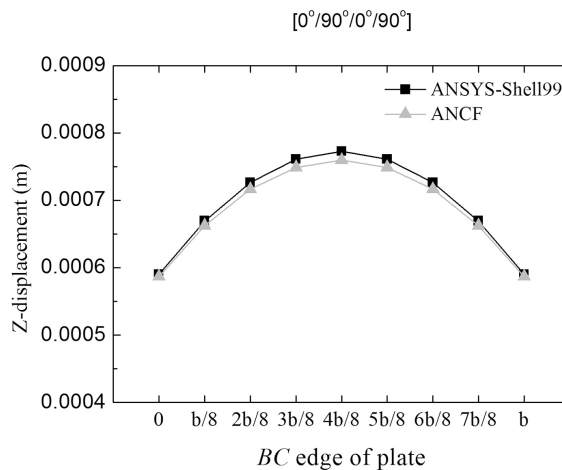


Fig. 4. Z-displacement at the edge *BC*.

Z. Shen & G. Hu

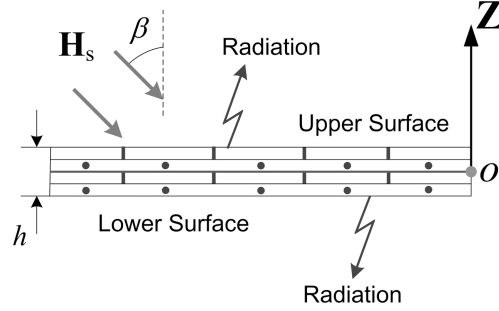


Fig. 5. Thermal analysis model of a laminated plate.

in Fig. 5. The upper surface of the plate will absorb the solar radiation heat flow \mathbf{H}_s and emit the heat flow to space by radiation, and the lower surface of the plate will only emit heat to space. The space temperature is assumed to be 4K, it is assumed that there is no heat transfer along the length and width of the plate, therefore the heat will only flow through the thickness of the plate [Johnston and Thornton, 2000; Dennehy *et al.*, 1990]. The transient heat conduction equation is then given by

$$\rho^{(k)} c_p^{(k)} \frac{\partial T(z, t)}{\partial t} = \lambda^{(k)} \frac{\partial^2 T(z, t)}{\partial z^2}, \quad (18)$$

where $\rho^{(k)}$, $c_p^{(k)}$ and $\lambda^{(k)}$ are the density, the specific heat and the thermal conductivity of the k th layer in the plate, respectively, and $T(z, t)$ is the temperature at point z and time t . The initial condition for the thermal model is assumed as follows:

$$T(z, t)|_{t=0} = T_0, \quad -\frac{h}{2} \leq z \leq \frac{h}{2}, \quad (19)$$

where $T_0 = 290$ K.

To solve the heat conduction problem, the boundary conditions have to be provided for the both surfaces of the plate. For the upper surface, the boundary condition is given by

$$-\lambda \frac{\partial T(z, t)}{\partial z} \Big|_{z=\frac{h}{2}} = \alpha_s Q_s - \varepsilon_T^{\text{up}} \sigma_T T^4(z, t) \Big|_{z=\frac{h}{2}}, \quad (20)$$

where α_s is the absorptance of material, $\varepsilon_T^{\text{up}}$ is the emittance of the upper surface, $\sigma_T = 5.669 \times 10^{-8} \text{ W/m}^2\text{K}^4$ is the Stefan-Boltzmann constant, and Q_s is the projected solar radiation to the upper surface, it will couple with the structural deformation of the plate.

$$Q_s = -\mathbf{n} \cdot \mathbf{H}_s, \quad (21)$$

where \mathbf{H}_s is the solar radiation heat flow and \mathbf{n} is the normal vector of the upper surface, which are shown in Fig. 6,

$$\mathbf{n} = \frac{\mathbf{r}_x \times \mathbf{r}_y}{|\mathbf{r}_x \times \mathbf{r}_y|}, \quad (22)$$

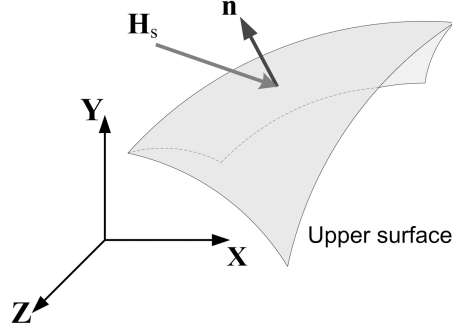


Fig. 6. Absorbed solar radiation on the upper surface.

where \mathbf{r}_x and \mathbf{r}_y are defined in Eq. (3) of the ANCF, and they will be obtained by absolute nodal coordinates \mathbf{e} for the considered point.

Similarly, the boundary condition of the lower surface is expressed as

$$-\lambda \frac{\partial T(z, t)}{\partial z} \Big|_{z=-\frac{h}{2}} = -\varepsilon_T^{\text{low}} \sigma_T T^4(z, t) \Big|_{z=-\frac{h}{2}}, \quad (23)$$

where $\varepsilon_T^{\text{low}}$ is the emittance of the lower surface.

To numerically solve the transient heat conduction problem, Eq. (18) is expressed in a finite element form with the initial and boundary conditions, this leads to

$$\mathbf{C}_p \dot{\mathbf{T}} + \mathbf{K}_c \mathbf{T} = \mathbf{R}_r(\mathbf{e}) + \mathbf{R}_T(\mathbf{T}), \quad (24)$$

where \mathbf{C}_p is the element lumped capacitance matrix and \mathbf{K}_c is the element conductance matrix, both are constant [Huebner and Thornton, 1982]

$$\mathbf{C}_p = \frac{\rho c_p A h_e}{2} \begin{bmatrix} 1 & 0 \\ 0 & 1 \end{bmatrix} \text{ (lumped)}, \quad \mathbf{K}_c = \frac{\lambda A}{h_e} \begin{bmatrix} 1 & -1 \\ -1 & 1 \end{bmatrix}, \quad (25)$$

where h_e is the element thickness, and A is the surface area of the plate.

The thermal loading vectors \mathbf{R}_r and \mathbf{R}_T are related to the geometry (or deformation) of the upper surface and the temperatures of the upper and lower surfaces, respectively, as shown below

$$\mathbf{R}_r^{\text{up}} = \alpha_s Q_s(\mathbf{e}) A \begin{bmatrix} 1 \\ 0 \end{bmatrix}, \quad (26)$$

where \mathbf{e} is the absolute nodal coordinate, it will change with the structural deformation and motion of the plate, and

$$\mathbf{R}_T^{\text{up}} = -\varepsilon_T^{\text{up}} \sigma_T A \begin{bmatrix} T_{\text{up}}(t)^4 \\ 0 \end{bmatrix}, \quad \mathbf{R}_T^{\text{low}} = -\varepsilon_T^{\text{low}} \sigma_T A \begin{bmatrix} 0 \\ T_{\text{low}}(t)^4 \end{bmatrix}, \quad (27)$$

where $T_{\text{up}}(t)$ and $T_{\text{low}}(t)$ are the temperatures of the upper and lower surfaces at time t , respectively.

Z. Shen & G. Hu

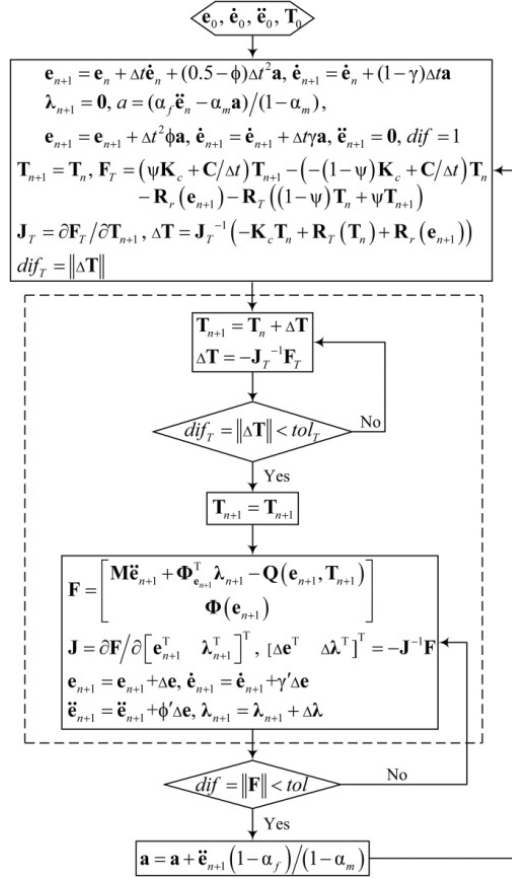


Fig. 7. The iteration procedure of the algorithm.

Finally, the coupled analysis between the thermal and structural responses is conducted by solving simultaneously Eqs. (17) and (24) with the proper initial and boundary conditions. The flow chart of the algorithm is shown in Fig. 7, where Δt is the time step-size, \mathbf{a} is an auxiliary variable, and $\alpha_m, \alpha_f, \phi, \gamma, \psi, \phi'$ and γ' are the numerical parameters [Huebner and Thornton, 1982; Arnold and Brüls, 2007]. The vectors λ and Φ are the Lagrange multipliers and the algebraic constraint equations, respectively, and $\Phi_{\mathbf{e}}$ is the Jacobian matrix of the constraints.

2.3.2. Numerical simulation

In this section, we will analyze a cantilevered solar panel suffered from a sudden solar radiation. The panel is made of upper and lower composite sheets and a hexagonal honeycomb core, as illustrated in Fig. 8(a), the geometry and material properties are given in Table 2. The absorptance is $\alpha_s = 0.79$ for the upper surface, the emittance of the upper and lower surfaces are $\varepsilon_T^{\text{up}} = 0.81$ and $\varepsilon_T^{\text{low}} = 0.86$

Thermally Induced Vibrations of Solar Panel

Table 2. Geometry and material of property of solar panel.

Property	Face sheet	Honeycomb core
Thickness h	2.54×10^{-4} m	0.0254 m
Density ρ	2800 kg/m ³	30 kg/m ³
Young's modulus		
E_{11}	68.9×10^9 N/m ²	0.41×10^9 N/m ²
E_{22}	68.9×10^9 N/m ²	0.24×10^9 N/m ²
E_{33}	68.9×10^9 N/m ²	0.24×10^9 N/m ²
Shear modulus		
$G_{12} = G_{13} = G_{23}$	25.9×10^9 N/m ²	0.15×10^9 N/m ²
Poisson's ratio		
$\nu_{12} = \nu_{13} = \nu_{23}$	0.33	0.3
CTE		
$\alpha_{11} = \alpha_{22} = \alpha_{33}$	2.32×10^{-5} /K	2.38×10^{-5} /K
Thermal conductivity λ	168 W/(m · K)	1.2 W/(m · K)

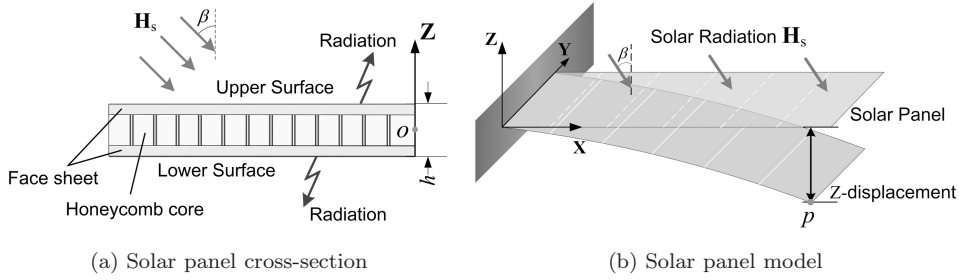
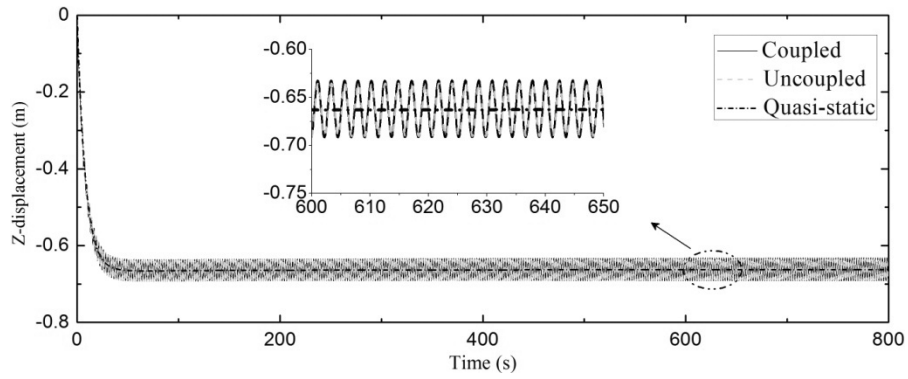


Fig. 8. Cantilevered solar panel.

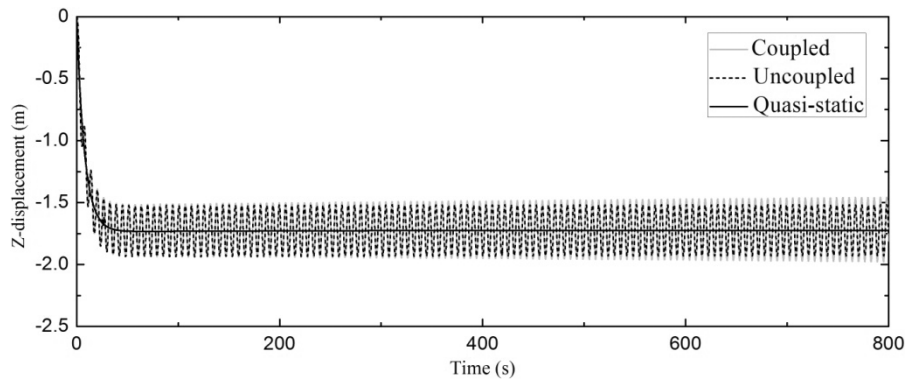
[Johnston and Thornton, 2000], respectively. In Fig. 8(b), the coupling between thermal and structural responses is illustrated, the absorbed heat from the upper sheet will depend on the structural deformation of the panel, and the solar radiation heat flux is $|\mathbf{H}_s| = 1350$ W/m². The coupled, uncoupled and quasi-static thermal-structural responses are calculated and the displacements in \mathbf{Z} -direction at the point p of the panel are shown in Figs. 9(a)–(c) for the different lengths of solar panels with an incident angle $\beta = 0^\circ$. The uncoupled thermal-structural analysis assumes that the absorbed heat flow is independent of structural deformation, and in the quasi-static thermal-structural analysis, the inertia term is ignored.

Compared to the quasi-static analysis, oscillatory responses are predicted if the inertia is included. The oscillation amplitude is larger when the coupling between the thermal and structural responses is considered, especially for long solar panels. The thermal flutter of the composite solar panel is also observed. It is induced due to the fact that the absorbed solar radiation heat flow is coupled with the deformation of the panel. The structural deformation will alter the absorbed heat flow from the upper surface, and the variation of the absorbed heat flow during the deformation will induce an oscillating temperature difference between the upper

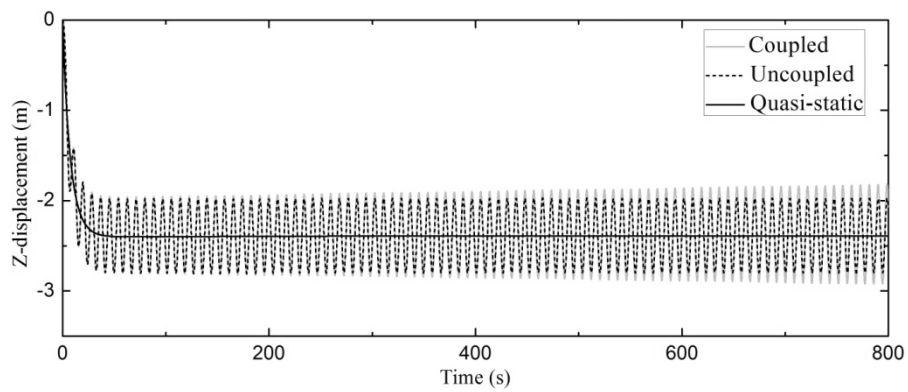
Z. Shen & G. Hu



(a) Solar panel with a length of 9 m



(b) Solar panel with a length of 15 m



(c) Solar panel with a length of 18 m

Fig. 9. TIVs response at the point p of a cantilevered solar panel.

Thermally Induced Vibrations of Solar Panel

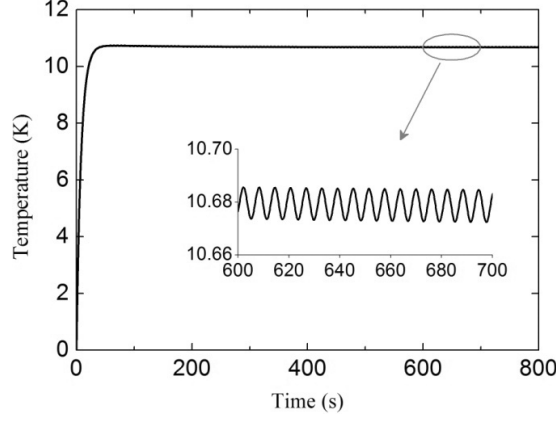


Fig. 10. Temperature difference between the upper and lower surfaces of the solar panel.

and lower surfaces, producing in turn an oscillating thermal torque in the solar panel. This phenomenon is more significant for long flexible panels. The oscillating temperature difference between the upper and lower surfaces of the panel is shown in Fig. 10 for the case of the coupled thermal and structural responses with a length of 15 m. It is seen that a small oscillation of temperature difference appears, its coupling with the structural deformation leads to the observed unstable vibration.

3. Coupled Dynamics Response Between Solar Panel and Satellite

3.1. NCF for satellite

In this section, we will analyze the coupling dynamic response between solar panel and satellite during an ellipse transition. The satellite is idealized as a rigid cylinder, and a natural coordinate formulation [Jalón and Bayo, 1994] is used to describe its motion. The main idea of the NCF is shown in Fig. 11, where $\mathbf{X}_1\mathbf{X}_2\mathbf{X}_3$ is the inertial Cartesian coordinate system and $\mathbf{x}_1\mathbf{x}_2\mathbf{x}_3$ is the local Cartesian body coordinate system. Two basic points l_1 and l_2 , and two unit vectors \mathbf{v} and \mathbf{w} are defined in the NCF, and the vector \mathbf{u} is defined based on the two basic points l_1 and l_2 , where $\mathbf{u} = \mathbf{r}^{g,l_2} - \mathbf{r}^{g,l_1}$. The three noncoplanar vectors \mathbf{u} , \mathbf{v} and \mathbf{w} form therefore a basis of a 3D space. Thus, the position vector of an arbitrary point p can be defined as follows:

$$\begin{aligned} \mathbf{r}^{g,p}(x_1, x_2, x_3, t) &= \begin{bmatrix} r_1^{g,p} \\ r_2^{g,p} \\ r_3^{g,p} \end{bmatrix} = [(1 - c_1)\mathbf{I} \quad c_1\mathbf{I} \quad c_2\mathbf{I} \quad c_3\mathbf{I}] \begin{bmatrix} \mathbf{r}^{g,l_1} \\ \mathbf{r}^{g,l_2} \\ \mathbf{v} \\ \mathbf{w} \end{bmatrix} \\ &= \mathbf{c}(x_1, x_2, x_3)\mathbf{q}^{g,p}(t), \end{aligned} \quad (28)$$

Z. Shen & G. Hu

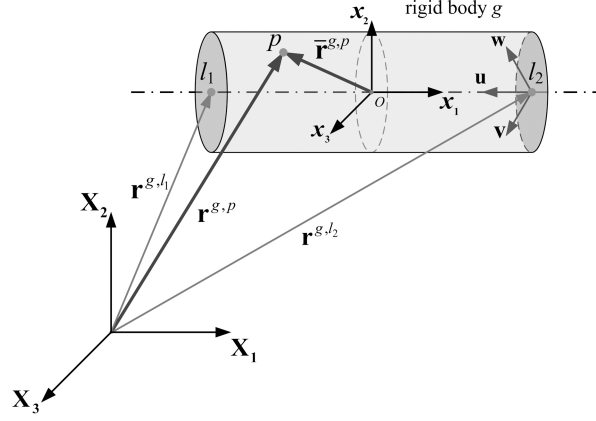


Fig. 11. Natural coordinate formulation.

where \mathbf{I} is the 3×3 identity matrix, c_1, c_2 and c_3 are the components of the vector $\mathbf{r}^{g,p} - \mathbf{r}^{g,l_1}$ in the basis formed by the vectors \mathbf{u}, \mathbf{v} and \mathbf{w} , and the matrix \mathbf{c} is only a position-dependent function in the local Cartesian body coordinate system and defined by the coefficients c_1, c_2 and c_3 . In the local Cartesian body coordinate system, the vector $\bar{\mathbf{r}}^{g,p} - \bar{\mathbf{r}}^{g,l_1}$ in the basis formed by vectors $\bar{\mathbf{u}}, \bar{\mathbf{v}}$ and $\bar{\mathbf{w}}$ can be defined as follows:

$$\bar{\mathbf{r}}^{g,p} - \bar{\mathbf{r}}^{g,l_1} = c_1 \bar{\mathbf{u}} + c_2 \bar{\mathbf{v}} + c_3 \bar{\mathbf{w}} = c_1 (\bar{\mathbf{r}}^{g,l_2} - \bar{\mathbf{r}}^{g,l_1}) + c_2 \bar{\mathbf{v}} + c_3 \bar{\mathbf{w}}. \quad (29)$$

Thus, the mass matrix is evaluated by [Jalón and Bayo, 1994]

$$\mathbf{M}^g = \rho^g \int_{V^g} \mathbf{c}(x_1, x_2, x_3)^T \mathbf{c}(x_1, x_2, x_3) dV^g, \quad (30)$$

where \mathbf{M}^g is also a constant matrix, ρ^g is the density of the rigid body, and V^g is the rigid body volume.

In a rigid-flexible multibody formulation, the system's mass matrix can be obtained directly by assembling the mass matrixes of a flexible body in the ANCF [Eq. (17)] and a rigid body in the NCF [Eq. (30)], respectively, and the system's elastic force comes only from the flexible body given by the ANCF. A rigid body and a flexible body can form a system by utilizing the kinematic constraints between rigid and flexible bodies.

3.2. Numerical applications

In the following, the method developed in Secs. 2 and 3.1 will be applied to analyze satellite dynamic responses during ellipse transitions. A simple satellite model consisting of a rigid hub and a flexible solar panel is shown in Fig. 12. The solar panel has a length of 9 m along the \mathbf{X} -direction and a width of 3 m along the \mathbf{Y} -direction, as shown in Fig. 8. The other parameters of the panel are the same as those in

Thermally Induced Vibrations of Solar Panel

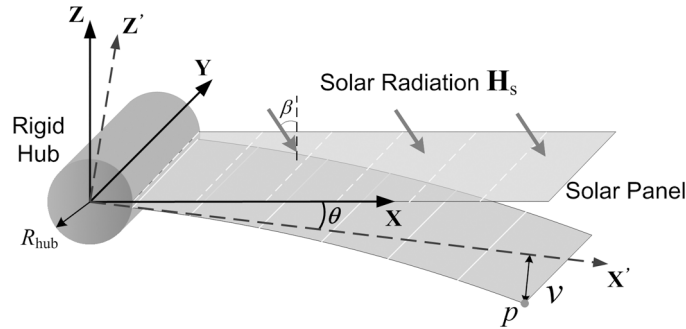
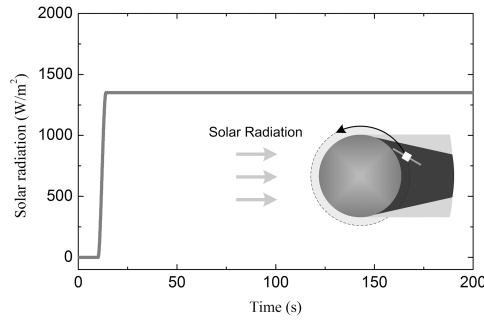
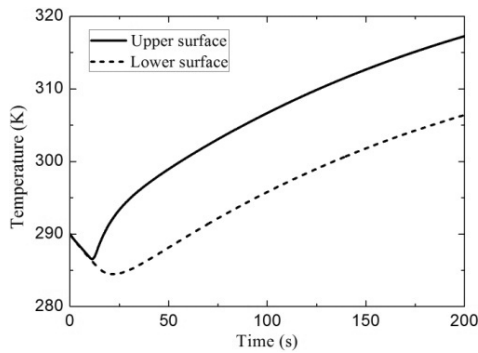


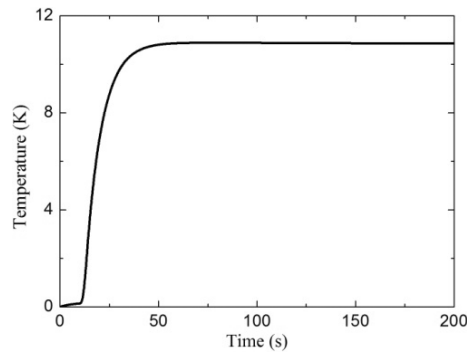
Fig. 12. A simple satellite model.



(a) Solar radiation during a sunrise orbital eclipse transition



(b) Surface temperatures



(c) Temperature difference

Fig. 13. Thermal response of the solar panel.

Sec. 2.3.2. The rigid hub has a mass 5000 kg, a radius of $R_{\text{hub}} = 1$ m and a length of 3 m.

The satellite is assumed to work in the low earth orbit, two situations are considered: in the first one, the panel suffers from a solar radiation during a sunrise orbital eclipse transition, as illustrated in Fig. 13(a), and in the second one, the

Z. Shen & G. Hu

panel suffers from a solar radiation during a sunset orbital eclipse transition, as shown in Fig. 15(a). For the first situation, the satellite is in the umbra region ($|\mathbf{H}_s| = 0 \text{ W/m}^2$) at the initial moment, and lies in horizontal direction with an incident angle $\beta = 0^\circ$, then the satellite enters into the penumbra region at $t = 10 \text{ s}$. It needs approximately 4 s to go through the penumbra region, and finally the satellite is exposed in the sunlight region ($|\mathbf{H}_s| = 1350 \text{ W/m}^2$). The loading of the solar radiation is also shown in Fig. 13(a).

In the computation, the solar panel is rigidly connected to the hub and the rigid hub has only one degree of freedom of the relative rotation around \mathbf{Y} -axis. NCF is used to describe the motion of the rigid hub and ANCF is used to describe the motion of the solar panel, respectively. The satellite dynamic response is computed for a duration of 200 s. The upper and lower surface temperatures and its difference are shown in Figs. 13(b) and 13(c), respectively. The temperature difference between the upper and lower surfaces is the main source of thermal torque, which induces the motion of satellite. It is seen that the temperature difference will be a constant after about 50 s, as shown in Fig. 13(c). The structural dynamic responses are presented in Fig. 14, more specifically, the displacement v of the point p with respect to the

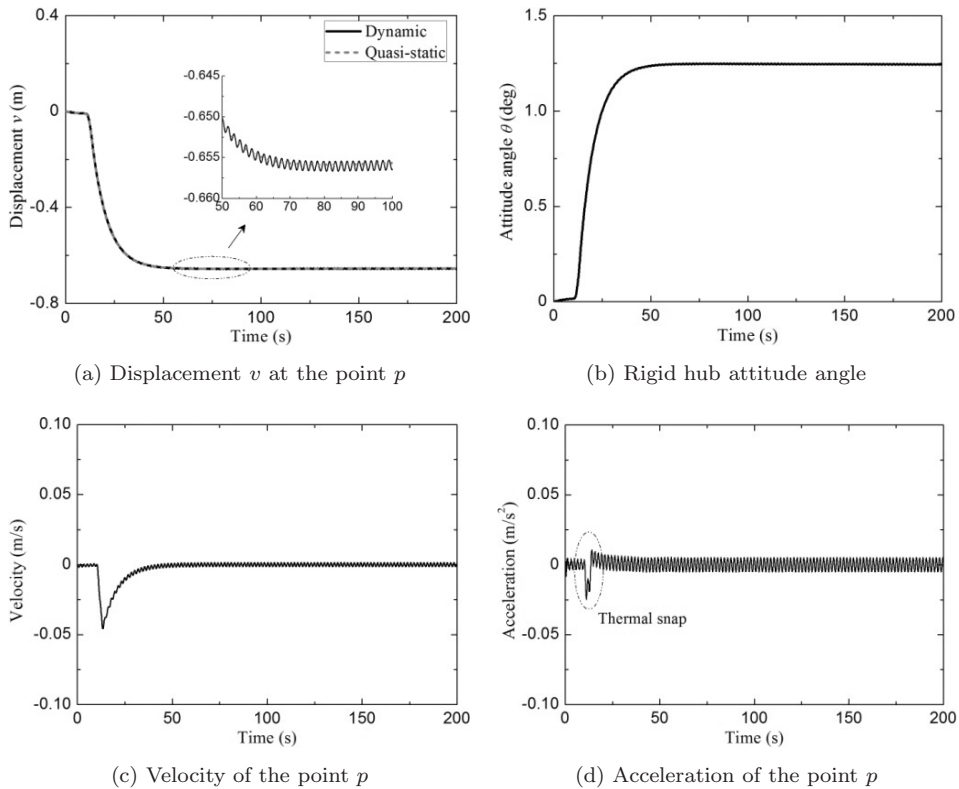
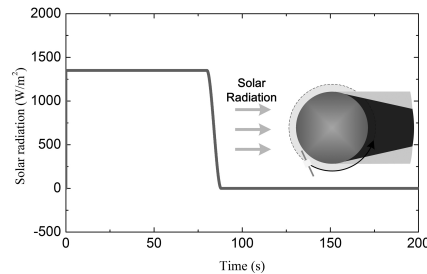


Fig. 14. Satellite dynamic response for the first situation.

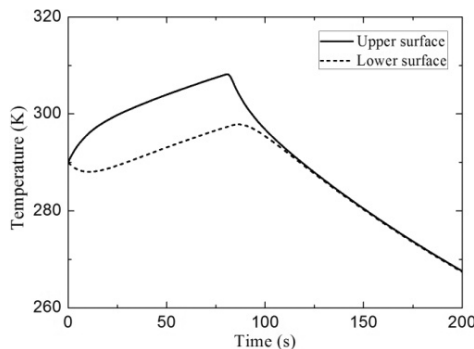
Thermally Induced Vibrations of Solar Panel

tangential reference frame ($\mathbf{X}'\mathbf{Y}\mathbf{Z}'$ in Fig. 12) as function of time is illustrated in Fig. 14(a). It is found that the dynamic response of the panel consists of a small oscillation superposed on the quasi-static response. Compare to Fig. 9(a), the oscillation amplitude is much smaller in the coupled response of the solar panel and satellite. The change of the rigid hub orientation is measured by the attitude angle θ (Fig. 12), and the computed result is given in Fig. 14(b). Although the rigid hub has a small time-varying attitude angle θ , it may cause the satellite to be unable to steady operation. The velocity and acceleration of the point p are also calculated and shown in Figs. 14(c) and 14(d), respectively, it is found that they both have peak values at about $t = 13.5\text{ s}$ and $t = 14.1\text{ s}$, separately, corresponding to the transition time from the penumbra to sunlight. The acceleration of the point p displays a thermal snap characteristic, which may be detrimental to high precision spacecraft operations, as observed during the UARS mission [Johnston and Thornton, 2000].

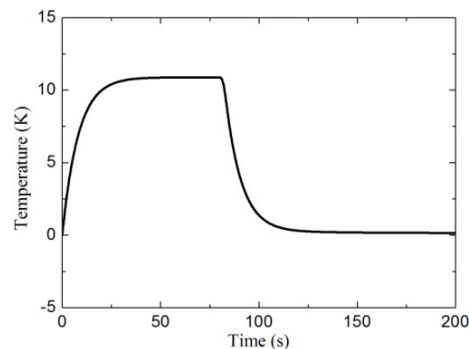
For the second situation, the sunset orbital eclipse transition is shown in Fig. 15(a), the satellite is suddenly exposed to the sunlight region with an incident angle $\beta = 0^\circ$ at $t = 0\text{ s}$, and enters into the penumbra region after 80 s. The satellite also spends 4 s to move into the umbra region. As shown in Fig. 15(b), the temperature peak value on the upper surface and the satellite transition to the



(a) Solar radiation during a sunset orbital eclipse transition



(b) Temperature on the solar panel



(c) Temperature difference

Fig. 15. Thermal response of solar panel.

Z. Shen & G. Hu

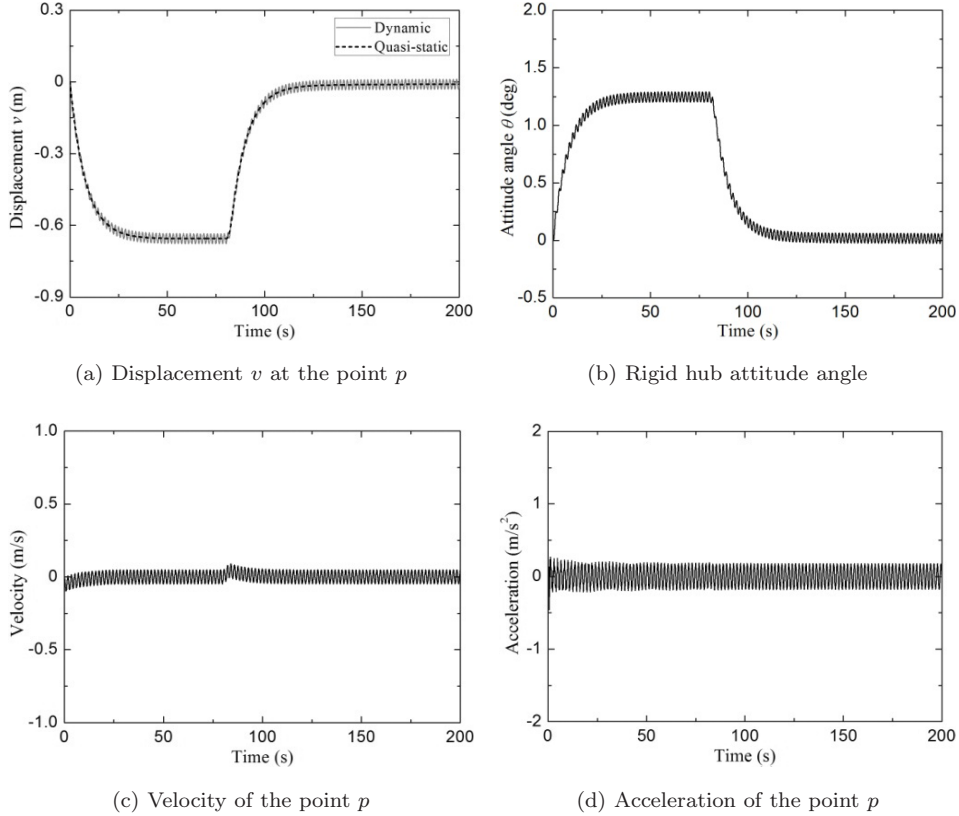


Fig. 16. Satellite dynamic response for the second situation.

penumbra region almost occur at the same time, however the temperature peak value of the lower surface has a delay due to the heat flow across the thickness, the temperature difference is also shown in Fig. 15(c). The structural dynamic responses are presented in Fig. 16. As shown in Fig. 16(a), the displacement response of the point p is quite different from that in the first situation [Fig. 14(a)], a net oscillation with large amplitude is observed. In addition, the rigid hub attitude angle θ also has a significant oscillation, as demonstrated in Fig. 16(b). Therefore, the satellite is more unstable when subjected to the solar radiation given in Fig. 15(a). The velocity of the point p has a small peak value occurring just after the satellite entering into the umbra region, which is about $t = 86.6$ s, as shown in Fig. 16(c). The acceleration of the solar panel is much larger compared to the first situation [Fig. 14(d)], but the thermal snap phenomenon is not observed for the second situation.

4. Conclusions

A laminated plate element with thermal effect is developed in the framework of absolute nodal coordinate formulation, it is then applied to examine the TIVs of a

Thermally Induced Vibrations of Solar Panel

composite solar panel. It is showed that thermal flutter can only be characterized with a coupled thermal and structural formulation, the thermal flutter is attributed to the oscillation of the temperature difference between the upper and lower surfaces of the panel and is more pronounced for longer flexible panels. The coupling response between solar panel and satellite during ellipse transitions is also analyzed by using the NCF for the rigid hub and the ANCF for the flexible solar panel. Two situations of solar radiation are considered, in the first case where the satellite escapes from the umbra region to the sunlight region, the numerical results show that a quasi-static response can be used instead of a dynamic one, and the thermal snap phenomenon is also discovered for the acceleration. For the second case, where the satellite escapes from the sunlight region to the umbra region, the TIVs are more pronounced and may result in instability for satellites.

Acknowledgments

The authors would like to thank Dr. Cheng Liu and Kai Zhang for their valuable suggestions. This work was supported by National Natural Science Foundation of China under Grants 10832002, 11290151 and 11221202.

References

- Arnold, M. and Brüls, O. [2007] “Convergence of the generalized- α scheme for the constrained mechanical systems,” *Multibody System Dynamics* **18**(2), 185–202.
- Bainum, P. M., Hamsath, N. and Krishna, R. [1989] “The dynamics and control of large space structures after the onset of thermal shock,” *Acta Astronautica* **19**(1), 1–8.
- Biswas, P. [1978] “Thermally-induced vibrations of a triangular slab resting on elastic foundation,” *Journal of Sound Vibration* **59**, 304–306.
- Boley, B. A. and Barber, A. D. [1957] “Dynamic response of beams and plates to rapid heating,” *Journal of Applied Mechanics* **24**, 413–416.
- Brischetto, S. [2009] “Effect of the through-the thickness temperature distribution on the response of layered and composite shells,” *International Journal of Applied Mechanics* **1**(4), 581–605.
- Chang, J. S., Wang, J. H. and Tsai, T. Z. [1992] “Thermally induced vibration of thin laminated plates by finite element method,” *Computers and Structures* **42**(1), 117–128.
- De Jalón, J. G. and Bayo, E. [1994] *Kinematic and Dynamic Simulation of Multibody Systems: The Real Time Challenge* (Spring-Verlag).
- Dennehy, C. J., Welch, R. V. and Zimbelman, D. F. [1990] “Sunrise/sunset thermal shock disturbance analysis and simulation for the TOPEX satellite,” *AIAA, 28th Aerospace Sciences Meeting*, Reno, Nevada.
- García de Jalón, J., Unda, J., Avello, A. and Jimenez, J. M. [1987] “Dynamic analysis of three-dimensional mechanisms in natural coordinates,” *Journal of Mechanisms, Transmissions, and Automation in Design* **109**(4), 460–465.
- Gerstmayr, J. and Shabana, A. A. [2005] “Efficient integration of the elastic forces and thin three-dimensional beam elements in the absolute nodal coordinate formulation,” *Multibody Dynamics 2005: ECCOMAS Thematic Conference, Madrid, Spain*.
- Gupta, A. K. and Singhal, P. [2010] “Effect of non-homogeneity on thermally induced vibration of orthotropic visco-elastic rectangular plate of linearly varying thickness,” *Applied Mathematics* **1**(4), 326–333.

Z. Shen & G. Hu

- Huebner, K. H. and Thornton, E. A. [1982] *The Finite Element Method for Engineers*, 2nd edn. (Wiley, Inc., New York).
- Jalón, D., García, J., Unda, J. and Avello, A. [1986] “Natural coordinates for the computer analysis of multibody systems,” *Computer Methods in Applied Mechanics and Engineering* **56**(3), 309–327.
- Johnston, J. D. and Thornton, E. A. [1998] “Thermally induced attitude dynamics of a spacecraft with a flexible appendage,” *Journal of Guidance Control and Dynamics* **21**, 581–587.
- Johnston, J. D. and Thornton, E. A. [2000] “Thermally induced dynamics of satellite solar panels,” *Journal of Spacecraft and Rockets* **37**(5), 604–613.
- Lal, A. and Singh, B. N. [2010] “Effect of uncertain system properties on thermo-elastic stability of laminated plates under nonuniform temperature distribution,” *International Journal of Applied Mechanics* **2**(2), 399–420.
- Li, W., Xiang, Z., Chen, L. and Xue, M. [2007] “Thermally flutter analysis of large-scale space structures based on the finite element method,” *International Journal for Numerical Methods in Engineering* **69**(5), 887–907.
- Mikkola, A. M. and Shabana, A. A. [2003] “A non-incremental finite element procedure for the analysis of large deformation of plates and shells in mechanical system applications,” *Multibody System Dynamics* **9**(3), 283–309.
- Reddy, J. N. [2004] *Mechanics of Laminated Composite Plates and Shells: Theory and Analysis* (CRC).
- Shabana, A. A. [1996] “An absolute nodal coordinate formulation for the large rotation and deformation analysis of flexible bodies,” Department of Mechanical and Industrial Engineering, University of Illinois at Chicago.
- Shabana, A. A. [2005] *Dynamics of Multibody Systems* (Cambridge University Press).
- Shabana, A. A. [2008] *Computational Continuum Mechanics* (Cambridge University Press).
- Tauchert, T. R. [1989] “Thermal shock of orthotropic rectangular plates,” *Journal of Thermal Stresses* **12**(2), 241–258.
- Thornton, E. A. and Foster, R. S. [1992] “Dynamic response of rapidly heated space structures,” *Computational Nonlinear Mechanics in Aerospace Engineering* **146**, 451–477.
- Tran, T. Q. N., Lee, H. P. and Lim, S. P. [2007] “Structural intensity analysis of thin laminated composite plates subjected to thermally induced vibration,” *Composite Structures* **78**(1), 70–83.
- Woodard, S. E. [1998] “Orbital and configuration influences on spacecraft dynamic response,” *Journal of Spacecraft and Rockets* **35**(2), 177–182.
- Xue, M. D., Duan, J. and Xiang, Z. H. [2007] “Thermally-induced bending-torsion coupling vibration of large scale space structures,” *Computational Mechanics* **40**(4), 707–723.
- Zhu, Z. H. and Morrow, B. [1998] “A novel computer simulator for cable-towed submerged vehicles,” in *Proceedings of the Second International Conference on Hydroelasticity in Marine Technology*, Fukuoka, Japan, December 1–3, pp. 293–306.
- Zhu, Z. H. and Pour, B. H. [2010] “A nodal position finite element method for plane elastic problems,” *Finite Elements in Analysis and Design* **47**(2), 73–77.
- Zimbelman, D. F., Dennehy, C. J., Welch, R. V. and Bom, G. H. [1991] “A technique for optimal temperature estimation for modeling sunrise/sunset thermal snap disturbance,” *Journal of Spacecraft and Rockets* **28**(4), 448–456.